Influence of the Structure of the Amino Group and Polarity of the Medium on the Photophysical Behavior of 4-Amino-1,8-naphthalimide Derivatives

Satyen Saha and Anunay Samanta*

School of Chemistry, University of Hyderabad, Hyderabad 500 046, India

Received: August 24, 2001; In Final Form: January 23, 2002

Photophysical behavior of two series of 4-amino-1,8-naphthalimide derivatives differing in the amino functionality has been studied as a function of the polarity of the medium. The location of the lowest singlet state of the systems, intramolecular charge transfer (ICT) in nature, is largely controlled by the conformation of the 4-amino group rather than its electron-donating ability. The fluorescence properties of the systems are strongly dependent on the nature of the amino group as well as on the polarity of the media. An increase in the length of the dialkyl groups connected to the amino nitrogen or an increase in the size of the ring containing the amino nitrogen enhances the nonradiative deactivation of the fluorescent state of the molecule. The nonradiative relaxation process is facilitated by an increase in the polarity of the media. The present results suggest that the radiationless deactivation of the fluorescent state of the systems is dependent on the nitrogen inversion rate at the amino group.

1. Introduction

Separation of charge is one of the most fundamental processes that forms the basis of numerous transformations of chemical and biological systems.[1−4] Electron donor−acceptor (EDA) molecules serve as ideal systems for the study of the charge-transfer process.[5] These molecules not only provide a testing ground for the contemporary theories of the electron-transfer process, but they also are useful for the study of solvation dynamics[6] and nonlinear optical properties.[7] Several fluorescent EDA molecules find use in laser applications[8] and as fluorescence probes in the study of the organized environments.[9,10]

The fluorescence efficiency of a molecular system is determined by the rate of the competing nonradiative deactivation of the fluorescent state. Very often, a structural change of the molecule in the excited state leads to an enhancement of the rate of the radiationless deactivation process. In the EDA systems, such as the coumarins, a low-lying nonfluorescent state with a twisted structure of the molecule has been proposed to account for an enhanced deactivation of the fluorescent state in polar media.[11−13] We have been studying the fluorescence behavior of several EDA systems with a view to understand the nonradiative deactivation mechanism or, more specifically, to determine whether an enhanced radiationless deactivation of a EDA system is linked to some structural changes of the molecule in the excited state.[14−16] These studies indeed revealed the presence of a nonfluorescent twisted intramolecular charge-transfer state,[17] similar to that proposed in the coumarins, is responsible for the deactivation of the fluorescent state of the aminophthalimides.[16] In the carbostyrils, which are structurally and electronically similar to the coumarins, we however found that the twisted state does not influence the fluorescence efficiency of the systems.[15] A more recent investigation on another series of EDA molecules revealed that the dependence of the nonradiative rate on the structure of the molecule and the polarity of the media could be best accounted for in terms of an inversion of the amino nitrogen rather than an internal rotation of the amino group in the excited state.[14] In this paper, we focus our attention on EDA systems, comprising various amino moieties as the electron donor and 1,8-naphthalimide as the common acceptor, with a view to find out whether the nature of the amino group (the electron donor) has any influence on the radiationless deactivation of the systems.

The naphthalimide derivatives have attracted the attention of the chemists, physicists, and biologists for various reasons. These are favorable coloring reagents in polymer industry,[18] they are well-known probes for medical and biological purposes such as local anesthetics,[19] and they possess antitumor properties;[20−22] they are potential HIV drugs,[23] fluorescent cell markers,[24] DNA-cleaving agents,[25,26] optical brighteners,[27] liquid-crystal additives,[28] and laser dyes.[29,30] These dyes also show interesting photophysical behavior in microheterogeneous media such as in micelle and cyclodextrin.[31]

Berces, Kossanyi, and co-workers extensively studied the spectroscopic and photophysical properties of various naphthalimide derivatives.[32−37] In some of these studies, the influence of the geometry of the molecule or intramolecular geometrical relaxation process on the emitting properties of the molecules has been investigated. *N*-Phenyl derivatives of naphthalimides exhibited dual fluorescence.[33,36,37] The short and the long wavelength components of the emission were attributed to fluorescence arising from a twisted and a planar phenyl group with respect to the naphthalimide moiety.

Brown and co-workers studied the photophysical properties of aminonaphthalimides in various media.[38,39] While the fluorescence yield of 4-aminonaphthalimide was as high as 0.8 in some media, the nonradiative deactivation of the fluorescent state was found to be quite efficient in aqueous solution.[39] The enhanced nonradiative rate in aquoeus media was attributed to the formation of a hydrogen-bonded cluster between the probe and solvent molecules. This group also studied the effect of pH of the medium on the fluorescence properties of aminonaphthalimides and explored possible use of these systems in fluorescence sensing of the transition-metal ions such as Cu^{2+}.[40]

* To whom correspondence should be addressed. E-mail: assc@uohyd.ernet.in.

10.1021/jp013287a CCC: $22.00
Published on Web 04/12/2002

CHART 1

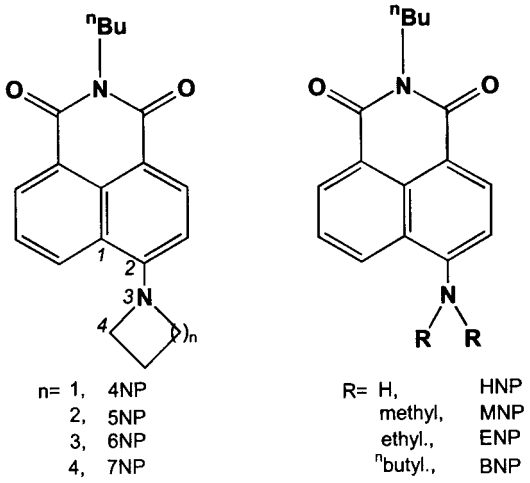

The photophysical behavior of the naphthalimides has also been studied by Pardo et al.[41−44] and ourselves.[45−47]

Taking into consideration the importance of the naphthalimide derivatives in biological applications, Redmond and co-workers recently studied the photochemical and photophysical behavior of a number of naphthalimides using fluorescence and flash-photolysis techniques.[48] In another recent paper, Dmitruk et al. invoked the involvement of a low-lying nonfluorescent charge-transfer state to account for a faster radiationless deactivation of the dimethylaminonaphthalimide relative to that of amino-naphthalimide.[49] This is very similar to what we proposed in the case of aminophthalimide derivatives.[16]

In this paper, we concentrate on two new series of 4-amino-1,8-naphthalimide derivatives, specifically synthesized to determine whether a minor variation of the amino functionality can influence the fluorescence efficiency or radiationless deactivation rate of these dye molecules. The imide hydrogen atom in these systems has been replaced by an *n*-butyl group to prevent the photochemical transformation such as proton transfer from complicating the fluorescence response of the molecules. The systems chosen in this study (Chart 1) can be classified into two sets. The first set comprises the parent molecule HNP and its dialkylated derivatives with different alkyl chain length. The second set, on the other hand, consists of systems in which the amino nitrogen is a part of a four- to seven-membered ring. The UV−vis absorption of the molecules is sensitive to the conformation of the amino moiety, and the fluorescence efficiency of the systems is strongly dependent on the structure of the amino group as well as on the polarity of the medium. The results suggest that inversion of the amino nitrogen acts as a nonradiative deactivation pathway in these systems.

2. Experimental Section

2.1. Materials. 4-Chloro-1,8-naphthalic anhydride (abbreviated as CNA, Acros), the starting material for the synthesis of the aminonaphthalimide derivatives (except HNP), was used as received. Trimethyleneimine (azetidine) and hexamethyleneimine from Fluka and dimethylamine (40 wt % solution in water) from Acros were used for synthesis without any further purification. Pyrrolidine and piperidine (Aldrich) and diethylamine and *n*-butylamine (Acros) were distilled prior to their use in the reaction. 4-Amino-1,8-naphthalimide (Aldrich) was used for the synthesis of HNP without any further purification. All solvents were rigorously purified prior to the fluorescence

SCHEME 1

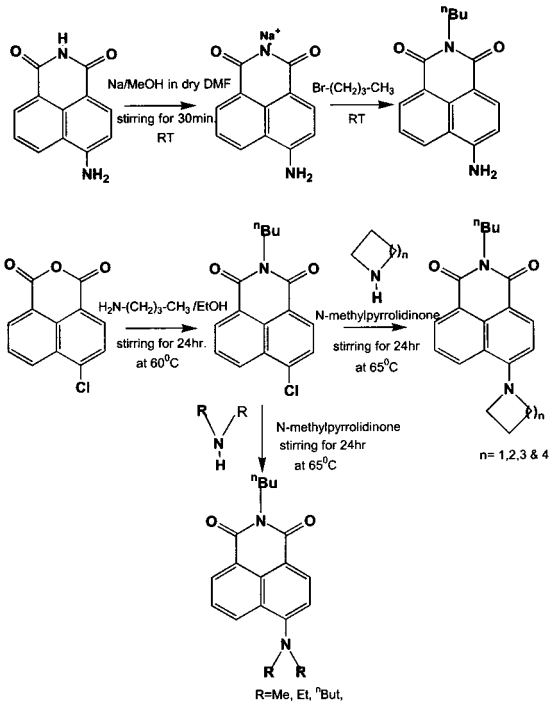

measurements by following standard procedures,[50] and it was confirmed by monitoring the long wavelength absorption maximum of the betaine dye that the solvents were almost free from polar impurities such as alcohol or water.[51]

2.2. Synthesis. The required derivatives (except HNP) were synthesized following a two-step procedure indicated in Scheme 1. In the first step, CNA was treated with *n*-butylamine to form 4-chloro-N-*n*-butyl-1,8-naphthalimide (CNM), which subsequently was treated with the appropriate amine to yield the desired product. The exact reaction conditions were as follows:

n-Butylamine (1.2 mmol) was added dropwise to a hot ethanolic solution of CNA (1 mmol) and stirred for 24 h at 60 °C. The product, CNM, was purified by column chromatography using a silica gel column and ethyl acetate in hexane as eluent.

In the second step, CNM (1 mmol) was dissolved in a minimum volume of *N*-methylpyrrolidinone, which was a better aprotic solvent for this type of nucleophilic displacement reaction,[52] and the appropriate amine (1.5 mmol) was added slowly with stirring. The reaction mixture was then stirred at 65 °C for 24 h. The excess amine and *N*-methylpyrrolidinone were removed through high vacuum, and the residue was washed with water and extracted with chloroform. The product was purified through a silica gel column using ethyl acetate and hexane mixture as eluent.

HNP was synthesized starting with 4-amino-1,8-naphthalimide, procured from Aldrich. The imide proton was removed by MeONa base, which was produced in situ following a reaction between Na and MeOH in dry DMF. The sodium salt of 4-amino-1,8-naphthalimide (1 mmol) so formed was allowed to react with 1-bromobutane (1.5 mmol), added dropwise. The product was purified by passing through a long neutral alumina column and by using 80% ethyl acetate in hexane as eluting agent. The analytical data for the final products (given below) confirm the structure of the compounds.

4NP. NMR data ($CDCl_3$): δ8.55(d, 1H), 8.4(d, 1H), 8.2(d, 1H), 7.5(t, 1H), 6.4(d, 1H), 4.5(t, 4H), 4.2(t, 2H), 2.6(p, 2H), 1.7(p, 2H), 1.45(m, 2H), 1.0 (t, 3H).

IR (KBr, cm^{-1}): 2955, 1676, 1639, 1375, 1348.

MP: 140−142 °C.

5NP. NMR data ($CDCl_3$): δ8.5(d, 2H), 8.3(d, 1H), 7.5(t, 1H), 6.75(d, 1H), 4.15(t, 2H), 3.75(t, 4H), 2.05(m, 4H), 1.7(p, 2H), 1.4(m, 2H), 0.95(t, 3H).

IR (KBr, cm^{-1}): 2955, 1680, 1637, 1398, 1348.

MP: 125 °C.

6NP. NMR data ($CDCl_3$): δ8.5(m, 2H), 8.35(d, 1H), 7.65(t, 1H), 7.15(d, H), 4.15(t, 2H), 3.2(t, 4H), 1.85(m, 4H), 1.7(m, 4H), 1.4(m, 2H), 0.95(t, 3H).

IR (KBr, cm^{-1}): 2935, 1697, 1651, 1390, 1344.

MP: 118−120 °C.

7NP. NMR data ($CDCl_3$): δ8.55(d, 1H), 8.45(d, 2H), 7.6(t, 1H), 7.15(d, 1H), 4.15(t, 2H), 3.55(t, 4H), 1.95(m, 4H), 1.8(m, 6H), 1.45(m, 2H), 1.0(t, 3H).

IR (KBr, cm^{-1}): 2957, 1689, 1647, 1394, 1344.

MP: 105 °C.

HNP. NMR data ($CDCl_3$): δ8.6(d, 1H), 8.4(d, 1H), 8.1(d, 1H), 7.7(t, 1H), 6.9(d, 1H), 5.0(s, 2H), 4.15(t, 2H), 1.7(m, 2H), 1.5(m, 2H), 1.0(t, 3H).

IR (KBr, cm^{-1}): 3433, 3362, 2955, 1672, 1637, 1398, 1307.

MP: 172 °C.

MNP. NMR data ($CDCl_3$): δ8.4(m, 3H), 7.6(dd, 1H), 7.05-(d, 1H), 4.15(t, 2H), 3.1(s, 6H), 1.7(qui, 2H), 1.4(m, 2H), 1.0-(t, 3H).

IR (KBr, cm^{-1}): 2959, 1684, 1641, 1388, 1350.

MP: 110 °C.

ENP. NMR data ($CDCl_3$): δ8.5(m, 3H), 7.6(t, 1H), 7.2(d, 1H), 4.15(t, 2H), 3.4(m, 4H), 1.7(m, 4H), 1.5(m, 4H), 1.2(t, 3H), 1.0(t, 3H).

At RT, viscous liquid.

BNP. NMR data ($CDCl_3$): δ8.5(m, 3H), 7.65(t, 1H), 7.2(d, 1H), 4.15(t, 2H), 3.35(t, 4H), 1.6(m, 12H), 0.95(m, 9H).

IR (KBr, cm^{-1}): 2957, 1693, 1657, 1390, 1356.

At RT, viscous liquid.

2.3. Apparatus and Methods. The fluorescence quantum yields of the systems were measured using quinine sulfate as the reference compound ($\phi_f = 0.546$ in 1 N H_2SO_4).[53] Dilute solutions with OD $\approx$ 0.05 at the excitation wavelength (which typically corresponded to a concentration in the micromolar range) were used for the quantum yield measurements. Optically matched solutions of the sample and reference were used. The fluorescence spectra for the sample and the reference compound were measured under the same operating conditions and settings. The quantum yields were measured by comparing the areas underneath the fluorescence spectra, measured using a standard software that came with the spectrofluorimeter. All fluorescence spectra were corrected for the instrumental response and each measurement was repeated twice.

The absorption and fluorescence spectra were recorded on a Shimadzu (UV-3101PC) spectrophotometer and SPEX (Fluoro-Max-3) spectrofluorimeter, respectively. The fluorescence decay curves were recorded using a IBH (5000U) single-photon-counting spectrofluorimeter. The instrument was operated with a thyratron-gated flash lamp filled with hydrogen at a pressure of 0.5 bar. The lamp was operated at a frequency of 40 kHz and the pulse width of the lamp under the operating conditions was ~1.2 ns. The decay times were estimated from the measured fluorescence decays and the lamp profile using a nonlinear least-squares iterative fitting procedure.[54] The goodness of the fit was evaluated from the χ^2 values and the plot of the residuals.

The IR and ^{H}NMR spectra were recorded on a JASCO (5300) FT-IR and a Bruker (ACF-200) spectrometer (200 MHz), respectively. The NMR measurements were performed in $CDCl_3$ at 25 °C.

The crystal structures of the two systems (5NP and 6NP) were determined using an Enraf-Nonius single-crystal diffractometer (MACH 3), using CAD-4 software (version 5.0). Data reduction, structure solution, and refinement were made using XTAL3.5, SHELXS-97,[55] and SHELXL-97[56] software, respectively.

Cyclic voltammetric measurements were carried out in acetonitrile with the help of a computer-driven potentiostat (CH Instrument, Model 620A). Scan rate was kept 0.1 V s^{-1} for all compounds. The estimated error for the potentiostat was $\pm$1 mV and the maximum estimated error associated with each measurement was $\pm$ 10 mV. The working electrode was a platinum electrode and the auxiliary electrode was a platinum wire. All redox potential values were measured with respect to the Ag/AgCl electrode. Tetrabutylammonium perchlorate (10^{-1}M) was used as the supporting electrolyte. The concentrations of the compounds were kept around 10^{-3} M and the solutions were deoxygenated before measuring potentials. All measurements were repeated twice.

The change in the molecular structure on electronic excitation has been assessed following a method suggested by Rettig and Maus.[57] According to this method, the ratio of the square of the transition dipole moments for the absorption and fluorescence serves as an indicator of the geometry change associated with electronic excitation (*vide* Discussion for details). To estimate the transition dipole moment (M_a) for the lowest energy absorption band from the experimentally obtained absorption spectrum, eq 1 is used[58]

$$M_a^2 = f(n)\frac{3hc2303}{8\pi^3 Nn}\int\frac{\epsilon(\nu_a)d\nu_a}{\nu_a} \qquad (1)$$

where $f(n)$ is a function of solvent refractive index, h is Planck's constant, c is the velocity of light in a vacuum, N is the Avogadro number, n is the refractive index of the medium, ν_a is the wavenumber of absorption, and $\epsilon(\nu_a)$ is the decadic molar extinction coefficient. The value of $\int(\epsilon_a(\nu_a)/\nu_a)d\nu_a$was obtained from the absorptions spectrum.

Similarly, the fluorescence transition dipole moment (M_f) of the $S_1 \rightarrow S_0$ electronic transition can be calculated from eq 2[58]

$$M_f^2 = f(n)\frac{3h\phi_f\langle\nu_f^{-3}\rangle}{64\pi^4 n^3\tau_f} \qquad (2)$$

where ϕ_f and τ_f are the fluorescence quantum yield and lifetime of the compound, respectively. The term mean cubic wavenumber $\langle\nu_f^{-3}\rangle$ was obtained from the fluorescence spectrum, $I_f(\nu_f)$ according to the equation[58]

$$\langle\nu_f^{-3}\rangle = \frac{\int I_f(\nu_f)\nu_f^{-3}d\nu_f}{\int I_f(\nu_f)d\nu_f}$$

AM1 calculations have been carried out on a personal computer using Hyperchem package (release 5.0) obtained from Hypercube. Inc. The molecular geometry was optimized initially using a molecular mechanics program (MMX). This was followed by unrestricted optimazation of the molecular geometry using AM1 method. Both MMX and AM1 programs were part of the Hyperchem package.

3. Results and Discussion

3.1. Photophysical Behavior. *3.1.1. Absorption.* The UV−vis absorption spectra of the systems have been studied in various solvents of different polarity and the spectral data have

TABLE 1: Absorption and Emission Spectral Data of NP Derivatives in Different Solvents at Room Temperature[a]

	λ_{max}^{abs} (nm)						ϵ^b	λ_{max}^{ems} (nm)					
system	hex.[c]	diox[d]	THF [e]	ACN[f]	EtOH[g]	MeOH[h]	ACN[f]	hex.[c]	diox[d]	THF[e]	ACN[f]	EtOH[g]	MeOH[h]
HNP	389	411	420	413	437	433	10289		493	500	513	532	535
MNP	388	403	408	415	421	422	10882	476	500	508	528	522	524
ENP	390	405	410	415	424	420	9379	484	507	514	523	534	540
BNP	397	413	415	423	431	430	14182	486	510	522	539	536	540
4NP	413	429	433	440	450	447	15042	487	503	507	528	532	544
5NP	417	432	436	443	451	448	16913	482	497	503	523	528	536
6NP	386	397	400	406	413	411	9076	481	504	513	537	545	551
7NP	400	418	423	433	442	440	10263	483	515	528	530	533	537

[a] Emission spectra were measured after exciting the solutions at 435 nm. [b] Molar extinction coefficient (mol^{-1} cm^{-1} L) measured in acetonitrile at the respective absorption maxima. [c] Hexane ($E_T(30) = 31.0$). [d] 1,4-Dioxane ($E_T(30) = 36.0$). [e] Tetrahydrofuran ($E_T(30) = 37.4$). [f] Acetonitrile ($E_T(30) = 45.6$). [g] Ethanol ($E_T(30) = 51.9$). [h] Methanol ($E_T(30) = 55.4$).

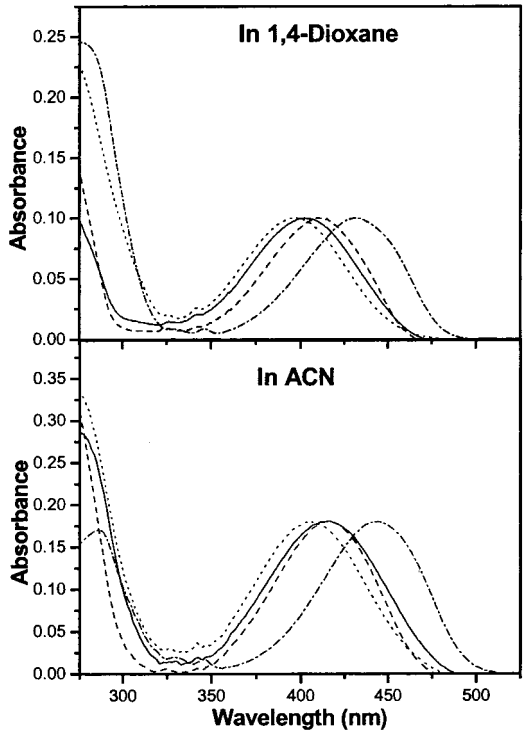

Figure 1. Absorption spectra of NP derivatives in 1,4-dioxane and acetonitrile (ACN) at 25 °C. (i) -•-•-•- 5NP; (ii) •••••• 6NP; (iii) − − − − HNP; (iv) —— MNP.

been collected in Table 1. A few representative spectra are shown in Figure 1. The longest wavelength absorption of the systems is characterized by a broad band with the maximum appearing between 385 and 450 nm. That this band arises because of an intramolecular charge transfer (ICT) between the 4-amino group to the naphthalimide ring system is evident from the following observations: the absorption is fairly broad (fwhm is typically 4500−5000 cm^{-1}) and intense (the molar extinction coefficient lies between 10000 and 15000 mol^{-1} cm^{-1} L), the peak position is rather sensitive to the polarity of the medium (*vide* Table 1), 4-unsubstituted naphthalimides do not exhibit this band,[45] and 4-amino-1,8-naphthalimide[38,39,47,59] and 4-methoxy-N-butyl-1,8-naphthalimide,[34] which possess an electron-donating group at 4-position, display a similar band.

As is typical of a charge-transfer transition, an increase in the polarity of the medium leads to a Stokes shift of the absorption maximum. A change of the solvent from hexane to acetonitrile typically results in 20−30 nm bathochromic shift of the absorption maximum of the systems. The magnitude of this shift suggests that the ground state of the molecules is significantly polar. Moreover, in HNP, specific hydrogen-bonding interaction in alcoholic solvent is perhaps responsible for an additional shift of ∼24 nm on changing the solvent from acetonitrile to ethanol.

The influence of the amino moiety on the energetics of the systems could be assessed from the spectral data presented in Table 1. Substitution of the amino hydrogens of the parent system, HNP, by two alkyl groups is expected to enhance the charge separation in the molecule because of the inductive effect of the alkyl groups. This should lead to a Stokes shift of the absorption maximum. Surprisingly, however, the band maxima observed for the linear dialkylamino derivatives are blue-shifted with respect to those of HNP in most of the solvents. A second interesting influence of the amino functionality is that the absorption peak position for 6NP is unusually blue-shifted relative to that of the other cyclic amino systems in any given solvent.

The molar extinction coefficients of the systems in acetonitrile at the respective absorption maxima have also been tabulated in Table 1. The molar extinction coefficient for 6NP is the lowest, and the maximum value has been observed for 5NP.

3.1.2. Fluorescence Spectra. Fluorescence spectra of the systems were recorded in various solvents of different polarity. The wavelengths corresponding to the fluorescence peaks are collected in Table 1 and a few representative spectra are shown in Figure 2. The fluorescence spectra of the systems consist of one broad band except in hexane, where some structure could be observed.

An increase in the polarity of the medium leads to a Stokes shift of the fluorescence maximum. The effect of the polarity of the medium on the fluorescence maximum is more pronounced than that on the absorption maximum. This is evident from the data presented in Table 1. While a change of the solvent from hexane to acetonitrile leads to a shift of the absorption maximum of a given system by around 25 nm, the magnitude of the spectral shift is twice as large in the fluorescence. This observation suggests that the emitting state of the systems is more polar than the ground state.

Unlike that observed in the absorption, the nature of the amino group seems to have little influence on the position of the fluorescence maxima. The fluorescence spectral data presented in Table 1 also indicate that hydrogen-bonding interaction with the solvent is significant only in HNP. The large red shift of the spectral maxima on changing the solvent from acetonitrile to ethanol is clearly the result of the hydrogen bonding. This effect, however, could not be observed with the other derivatives.

3.1.3. Fluorescence Quantum Yield. Fluorescence quantum yields (ϕ_f) of the systems, measured in a series of solvents of different polarity, are collected in Table 2. These data can be summarized as follows:

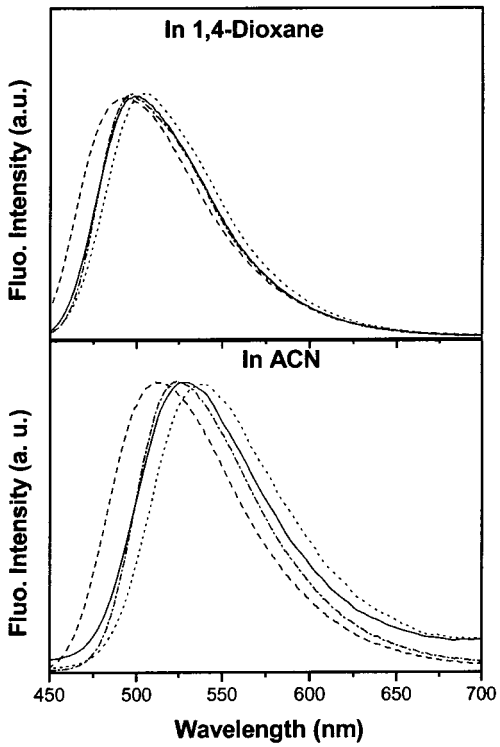

Figure 2. Fluorescence spectra of NP derivatives in 1,4-dioxane and acetonitrile (ACN) at 25 °C. (i) -•-•-•- 5NP; (ii) •••••• 6NP; (iii) – – – – HNP; (iv) —— MNP. Emission spectra were recorded after exciting the solutions at 435 nm. Spectra were corrected for instrument response and normalized at their respective peak maximum.

TABLE 2: Fluorescence Quantum Yields[a] of the Aminonaphthalimides at Room Temperature

system	hexane[b]	dioxane[c]	THF[d]	ACN[e]	EtOH[f]	MeOH[g]
HNP		0.76	0.86	0.77	0.58	0.48
MNP	0.82	0.76	0.50	0.05	0.01	0.01
ENP	0.78	0.41	0.15	0.02	0.01	0.01
BNP	0.78	0.50	0.32	0.03	0.01	0.006
4NP	0.86	0.80	0.79	0.83	0.72	0.60
5NP	0.80	0.78	0.66	0.12	0.04	0.03
6NP	0.76	0.74	0.60	0.07	0.01	0.01
7NP	0.94	0.32	0.13	0.01	0.01	0.01

[a] With a measurement error of ±10%. [b] Hexane ($E_T(30) = 31.0$). [c] 1,4-Dioxane ($E_T(30) = 36.0$). [d] Tetrahydrofuran ($E_T(30) = 37.4$). [e] Acetonitrile ($E_T(30) = 45.6$). [f] Ethanol ($E_T(30) = 51.9$). [g] Methanol ($E_T(30) = 55.4$).

Except for the first member of each group, HNP and 4NP, the fluorescence quantum yield (ϕ_f) decreases with an increase in the polarity of the medium. The decrease is most prominent in a polar environment. In HNP, the hydrogen-bonding interaction is presumably responsible for an additional drop of the quantum yield in alcoholic solvents.

The influence of the amino group on the fluorescence efficiency of the systems is clearly evident from the data presented in Table 2. In polar media, as the ring size containing the amino nitrogen is increased, the yield drops sharply. For example, a 76-fold decrease in yield occurs when the ring size is increased from 4 to 7 in acetonitrile. In the linear amino systems, a 52-fold drop of fluorescence intensity could be observed in acetonitrile. In a less polar environment, the trend is very similar, though the magnitude of the change is not as pronounced.

3.1.4. Fluorescence Decay Behavior. The fluorescence decay behavior of the systems have been studied in several solvents of different polarity and the data have been presented in Table 3. Typical decay profiles along with the autocorrelation diagrams are shown in Figure 3.

TABLE 3: Fluorescence Decay Times (τ_f)[a] (in ns) for the Systems in Various Solvents of Different Polarity

systems	hexane	1,4-dioxane	THF	ACN	EtOH
HNP		11.1	10.8	11.2	8.9
MNP	7.1	9.2	6.2	0.8 (98)	0.2 (98)
				10.5 (2)	8.9 (2)
ENP	7.5	6.7	2.7 (96)	0.3 (92)	0.04 (99)
			9.4 (4)	10.6 (8)	9.2 (1)
BNP	8.1	8.3	5.7	0.7 (91)	0.1 (99)
				10.4 (9)	9.1 (1)
4NP	6.8	9.4	9.0	10.0	9.6
5NP	6.7	9.0	7.4	1.2 (98)	0.2 (99)
				9.0 (2)	8.6 (1)
6NP	7.3	9.4	8.4	1.1 (99)	0.2 (99)
				9.9 (1)	5.7 (1)
7NP	7.5	5.8	2.5 (96)	0.2 (97)	
			8.8 (4)	9.7 (3)	

[a] The solutions were excited at the respective absorption maxima and fluorescence decays were measured at the corresponding fluorescence peak maxima of the compounds. Biexponential fitting was resorted when single-exponential fitting was not satisfactory. The quantities in the bracket indicate the relative weight of each component.

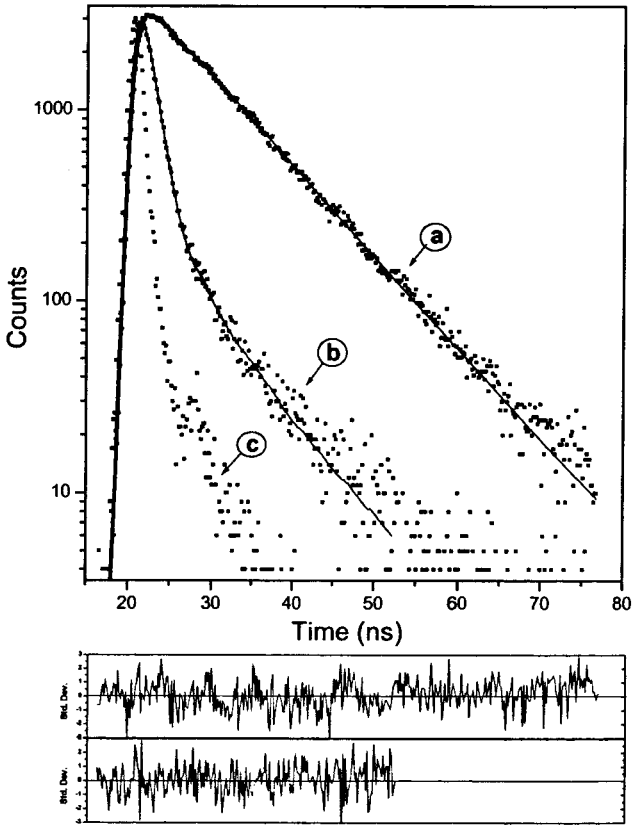

Figure 3. Fluorescence decay curves for 5NP in (a) 1,4-dioxane and (b) acetonitrile. Solutions were excited at 430 nm and emission was monitored at the emission maximum. The solid lines represent the best fit to the data. The instrumental response function (lamp profile) is also shown in (c). The weighted deviations are shown below the decay curves. The decay parameters are indicated in Table 3.

4NP and HNP exhibit single-exponential decay in all solvents irrespective of the polarity. Even in alcoholic solvents, a single-exponential behavior is observed. Of the two derivatives, HNP has a higher fluorescence decay time (τ_f) in all solvents except in alcoholic solvents, where hydrogen-bonding interaction reverses the trend. For higher members of both the series, the effect of polarity is very similar to what is observed for the

TABLE 4: Radiative (k_f) and Nonradiative (k_{nr}) Rate Constant[a] for the NP Derivatives in Various Solvents at Room Temperature

	k_f (10^7 s^{-1})					k_{nr} (10^7 s^{-1})				
system	hex.	diox.	THF	ACN	EtOH	hex.	diox.	THF	ACN	EtOH
HNP		6.81	8.02	6.90	6.58		2.17	1.25	2.00	4.63
MNP	11.56	8.20	8.09	6.49	3.53	2.59	2.63	7.96	120.7	388.6
ENP	10.36	6.11	5.71	5.47	17.5	2.92	8.72	31.60	359.50	2483.1
BNP	9.55	6.03	5.62	4.58	15.25	2.72	6.01	11.77	138.50	1680.2
4NP	12.73	8.47	8.86	8.35	7.56	2.04	2.14	2.30	1.66	2.88
5NP	12.02	8.70	8.97	9.91	19.60	3.02	2.42	4.56	74.12	482.9
6NP	10.40	7.56	7.19	6.13	5.17	3.28	3.03	4.76	84.05	570.6
7NP	12.60	5.57	5.18	6.47		0.84	11.7	34.66	581.8	

[a] The rate constants were evaluated from the measured ϕ_f and τ_f values using $k_f = \phi_f/\tau_f$ and $k_{nr} = (1 - \phi_f)/\tau_f$. In a biexponential decay behavior, the τ_f value of the major component was used in the calculations.

fluorescence quantum yield. Increase in the polarity of the medium leads to a shortening of the lifetime.

The influence of the structure of the amino group is also similar to that observed in the fluorescence quantum yield. The lifetime is shorter for the higher members and the decrease in lifetime with increase in the member size is more pronounced in a polar environment. A minor component (1−9%) with a relatively long lifetime could be observed for most of the members (excluding the first one) in the polar media. For example, in 5NP, the fluorescence decay is single exponential in THF but clearly biexponential in ACN. On the other hand, in 6NP or 7NP, the decay behavior is biexponential even in THF.

3.1.5. Nonradiative Rate Constant. The radiative (k_r) and nonradiative (k_{nr}) rate constants of the systems in different solvents, evaluated from the measured values of ϕ_f and τ_f using $k_r = \phi_f/\tau_f$ and $k_{nr} = (1 - \phi_f)/\tau_f$, are collected in Table 4.

As can be seen, the radiative rate constants of the various systems do not depend on the nature of the amino moiety. Instead, these values cluster within a narrow range. Except for the fact that these values are relatively higher in hexane, no other solvent dependence could be observed in aprotic media. Even though the polarity of the medium has very little influence on the k_{nr} values of HNP and 4NP, the effect of the medium is rather dramatic on the k_{nr} values of the higher members. In 5NP, nearly 30-fold increase in the nonradiative rate constant could be observed on changing the solvent from 1,4-dioxane to acetonitrile. This factor is even higher (50-fold) in 7NP. Polarity-assisted nonradiative decay is also quite pronounced in the linear chain derivatives. The factor by which the k_{nr} value is increased on changing the solvent from 1,4-dioxane to acetonitrile is 46 and 41 for MNP and ENP, respectively.

The influence of the structure of the amino group on the magnitude of the nonradiative rate constant is quite dramatic. In polar media such as in acetonitrile, where the structural effect is most pronounced, the k_{nr} value for 7NP is higher than that of 4NP by a factor of 363. Among the linear amines, the k_{nr} value is the highest for ENP. This value is 180-fold higher than that of HNP. The combined influence of the polarity of the medium and the amino group on the nonradiative rate constants of the systems is pictorially depicted in Figure 4. While the k_{nr} values of the different systems follow a systematic trend, ENP, for reasons not clear to us at present, shows the highest values among the linear chain systems.

3.2. AM1 Calculation, Crystallographic Data, Cyclic Voltammetric Data. AM1 calculations have been carried out for all the systems to find out the optimized geometry of the molecules and the dipole moments of the systems. The C(2)−N(3) bond length (Chart 1, henceforth, simply referred to as C−N bond) of the various systems and the ground-state dipole

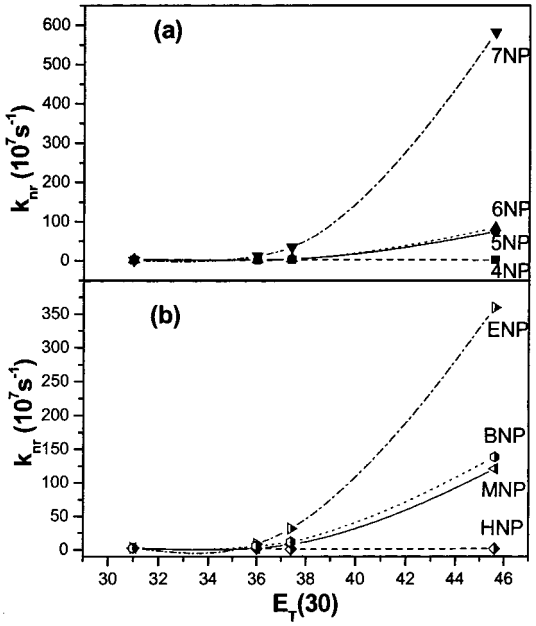

Figure 4. Influence of polarity of the medium and the amino group on the nonradiative rate constants of the systems: (a) for ring systems, (b) for linear chain derivatives. Solvents used are hexane ($E_T(30) = 31.0$), 1,4-dioxane ($E_T(30) = 36.0$), tetrahydrofuran ($E_T(30) = 37.4$), acetonitrile ($E_T(30) = 45.6$).

TABLE 5: AM1 Calculated Ground-State Dipole Moment (μ_g) and C−N Bond[a] Length in Å for Various NP Derivatives

compounds	μ_g (D)	r_{CN}[a]
HNP	6.23	1.3812
MNP	5.39	1.4196
ENP	5.45	1.4227
BNP	5.34	1.4251
4NP	6.35	1.3977
5NP	5.52	1.4238
6NP	4.83	1.4293
7NP	6.24	1.4054

[a] C2−N3 bond in Chart 1.

moment of the systems are presented in Table 5. The crystal structures of the systems were determined where possible with a view to correlate the structure factor with the photophysics of the molecules. Among the aminonaphthalimides, good single crystal suitable for X-ray crystallography could only be obtained for 5NP and 6NP (from absolute ethanol). The details of the crystal structure will be published elsewhere. The molecular information crucial to this investigation, as obtained from X-ray crystallography, has been summarized in Table 6. The redox behavior of the systems has been studied through cyclic

TABLE 6: Structural Parameters as Obtained from X-ray Crystallography

parameters	5NP	6NP
twist angle (degree)[a]	30.2 (5)	70.0 (9)
angles around the N (degree)[b]	110.6 (3)	109.4 (6)
	120.5 (3)	114.7 (5)
	127.1 (3)	116.3 (6)
C−N bond length (Å)[c]	1.371 (4)	1.388 (9)

[a] Torsion angle consisting atoms C1−C2−N3−C4 (see Chart 1). [b] Three angles around the nitrogen atom of amine. [c] Refers to C2−N3 bond.

TABLE 7: Reduction Potentials for the NP Derivatives

compounds	$-E^{1/2}_{red}$ (V)[a]
HNP	1.31
MNP	1.23
ENP	1.21
BNP	1.22
4NP	1.32
5NP	1.29
6NP	1.22
7NP	1.24

[a] The half-reduction potential.

voltammetry primarily to understand the spectral behavior of the molecules (*vide* later). While the oxidation behavior of almost all the systems is found irreversible, the reduction is quasi reversible in nature. The measured reduction potentials of the various systems have been collected in Table 7.

4. Discussion

4.1. Ground-State Conformation. The energy of the charge-transfer state of a EDA molecule is generally determined by the strength of the electron donor and acceptor moieties. Since a dialkylamino group is a better electron donor than the unsubstituted amino group (because of the inductive effect of the alkyl groups), one expects HNP to absorb at a higher energy relative to the remaining systems. Interestingly, MNP and ENP absorb at a higher energy compared to HNP. This anomalous behavior can only be accounted for if it is assumed that the dialkylamino moieties are twisted with respect to the naphthalimide ring. The repulsion between the alkyl groups and the *peri* hydrogens of the naphthalimide ring is likely to be the driving force for a twisted structure of the dialkylamines in the ground state.

Several other theoretical and experimental parameters confirm that supposedly better electron-donating dialkylamino moieties contribute less charge to the electron-deficient naphthalimide moiety. First, the C−N bond length, which is a measure of the charge separation, is calculated to be the lowest for HNP (Table 5). Second, the AM1 calculated ground-state dipole moment is much higher for HNP even though the molecule contains a relatively poorer donor. Third, the reduction potential, which is a measure of the electron deficiency of a system, is the lowest for HNP (Table 7).

A similar explanation can be used to account for the anomalous spectral data of 6NP. The absorption maxima for this system are significantly blue-shifted with respect to those of the other ring systems. AM1 calculations indeed confirm that the ground-state dipole moment of 6NP is significantly lower than that of the other ring systems. The C−N bond length in 6NP is the largest among all the members. The molar extinction coefficient of 6NP is measured to be the lowest. All these data support that the geometry of the amino nitrogen in 6NP is not favorable for charge separation in this EDA system. The reduction potential of 6NP is highest among all the cyclic derivatives. The crystal structure data of the systems (Table 6) also suggest that the C−N bond length in 6NP is higher than that in 5NP, the three angles around the amino nitrogen are more pyramidal in 6NP, and the twist angle (C1−C2−N3−C4, in Chart 1) is much higher for 6NP. These data are also consistent with the spectral behavior of the systems.

4.2. Excited-State Geometry. While the difference in the ground-state structure of the systems results in sharp difference in the absorption wavelength of the charge-transfer transition, interestingly, the difference in the emission wavelength of the various derivatives is rather small. This suggests that electronic excitation that leads to an enhancement of charge separation in the excited state (as evident from the influence of the polarity of the medium on the fluorescence maximum) makes the amino nitrogen almost planar in all cases thereby removing the difference in the structure of the molecules and its strong influence on the spectral properties of the system.

As one of the tools for determining the flattening of a structure on electronic excitation, Rettig and Maus recently suggested[57] that the ratio (r) of the square of the fluorescence transition dipole moment (M_f^2) to the square of the absorption transition dipole moment (M_a^2) can be employed as an indicator of the excited-state geometry. According to this procedure, an r value of larger than unity points to a better π-electron conjugation and hence, a flattening of the structure in the excited state. On the other hand, an r value of smaller than unity is indicative of a comparatively reduced transition moment to the ground state and hence, a twisting of the structure. The measured values of r (*vide* Experimental Section for procedure) for the present systems are higher than unity (e.g., 1.14 for 5NP and 1.27 for 6NP) confirming a more planar structure of the molecules in the excited state.

4.3. Excited-State Dipole Moment. Attempts were made to quantify the extent of charge separation on electronic excitation of the various systems by measuring the change in the dipole moment ($\Delta\mu = \mu_e - \mu_g$) utilizing the shift between the absorption and fluorescence maxima ($\Delta\bar{\nu} = \bar{\nu}_a - \bar{\nu}_f$) as a function of the solvent polarity.[60−62] According to Lippert−Mataga equation,

$$\bar{\nu}_a - \bar{\nu}_f = \frac{2(\mu_e - \mu_g)^2}{hca^3}\left[\frac{\epsilon - 1}{2\epsilon + 1} - \frac{n^2 - 1}{2n^2 + 1}\right] + \text{constant} \quad (3)$$

where $\bar{\nu}_a$ and $\bar{\nu}_f$ are the wavenumbers of the absorption and fluorescence maxima, μ_g and μ_e are the ground- and excited-state dipole moments, ϵ and n are the dielectric constant and refractive index of the medium, c is the velocity of light, and a is the Onsager cavity radius.

A plot of $\Delta\bar{\nu}$ versus Δf gives $\Delta\mu$ where

$$\Delta f = \frac{\epsilon - 1}{2\epsilon + 1} - \frac{n^2 - 1}{2n^2 + 1}$$

Even though we used 13 solvents to obtain the dipole moment change on excitation, the correlation between $\Delta\bar{\nu}$ and Δf was found to be rather poor (Figure 5I, correlation coefficient <0.8). Using the AM1 calculated longest distance between the carbonyl oxygen and amino nitrogen as the Onsager cavity radius ($3.647A^0$ for 5NP and $3.687A^0$ for 6NP), the dipole moment change on excitation is estimated to be around 3.5D and 4.1 D for 5NP and 6NP, respectively.

Since $\Delta\bar{\nu}$ is usually better correlated to the microscopic solvent polarity parameter, $E_T(30)$,[51] we have examined the

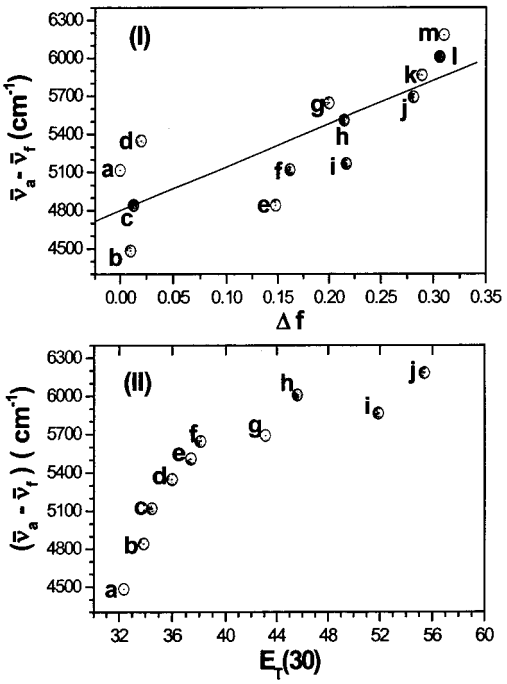

Figure 5. Dependence of Stokes' shift ($\bar{\nu}_a - \bar{\nu}_f$) of 6NP on the (I) solvent polarity function, Δf (see text). The straight line represents the best least-squares fit to the data. Solvents are (a) hexane, (b) carbontetrachloride, (c) toluene, (d) 1,4-dioxane, (e) chloroform, (f) diethyl ether, (g) ethyl acetate, (h) tetrahydrofuran, (i) dichloromethane, (j) butyronitrile, (k) ethanol, (l) acetonitrile, (m) methanol. (II) $E_T(30)$, solvents are (a) carbon tetrachloride; (b) toluene; (c) diethyl ether; (d) 1,4-dioxane; (e) tetrahydrofuran; (f) ethyl acetate; (g) butyronitrile; (h) acetonitrile; (i) ethanol; (j) methanol.

correlation between $\Delta\bar{\nu}$ and $E_T(30)$ following a recent equation suggested by Ravi et al.[63] Interestingly, the $\Delta\bar{\nu}$ versus $E_T(30)$ plot for 6NP (Figure 5II) clearly shows two slopes suggesting the involvement of more than one excited state in the photophysics of the molecule. Kosower found a similar type of dependency (two slopes in the $\bar{\nu}_f$ vs $E_T(30)$ plot) while investigating the excited-state intramolecular charge transfer for 8-(phenylamino)-1-naphthalenesulfonate and suggested the involvement of two excited states in photophysics.[64]

4.4. Nonradiative Rate and Molecular Dynamics. Among the linear members, the k_{nr} value is measured to be the lowest for HNP and highest for ENP. The large difference in the k_{nr} values of the systems, particularly in the polar media, cannot be attributed to the difference in the electron-donating abilities of the amino moieties as these are very similar in all the systems except in HNP. Hence, the difference in the k_{nr} values of the various systems arises because of a difference in the rate of some internal motion in the molecular systems. One can think of an internal rotation (twisting) around the C−N bond or an inversion of the amino nitrogen that may influence the k_{nr} values of the systems. For the ring systems, one needs to consider the ring inversion also as a possible internal motion. If internal rotation around the C−N bond was responsible for the nonradiative relaxation, then one would have expected a higher k_{nr} value for HNP or MNP as these systems contain a smaller rotating moiety. The experimental trend of the values of k_{nr} for the current systems clearly goes against this type of internal motion. Among the ring systems, the highest k_{nr} values have been obtained for the seven-membered ring system, though the internal rotation around the C−N bond is expected to be the slowest for this system. Obviously, internal rotation around the C−N bond cannot be considered to be the cause of the large difference in the rates of the nonradiative relaxation of the various systems.

Nitrogen inversion of the amino groups is another internal motion that is quite efficient in linear as well as in cyclic amines. The inversion of the amino nitrogen takes place via a transition state involving a planar nitrogen.[65] Hence, the substituents that can stabilize the planar transition state lower the inversion barrier. It is known that the N-inversion barrier in a diethylmethylamine is lower than that in trimethylamine.[66] It is also well-documented that a seven-membered cyclic amine has a lower barrier to inversion compared to the lower members.[65] The inversion barriers for the various tertiary amines are generally in the range of 6−19 kcal/mol.[67] However, substituents which can bring conjugation (such as $-NO_2$, $-CO$, etc.) with the amine reduce the inversion barrier to such a low value that cannot be measured by dynamic magnetic resonance spectroscopy,[67] a technique extensively used for the study of the inversion barrier. In the present systems, charge transfer through the π-network (which is convincingly established) is expected to make the inversion process highly efficient. This conjugation makes the internal rotation around the C−N bond far more difficult than in systems where such conjugation is not available. What transpires from the above discussion is that the k_{nr} values of the systems are more in accordance with the N-inversion rate of the various amino moieties than with internal rotation. A rather small difference in the k_{nr} values of 5NP and 6NP is consistent with a similar magnitude of the N-inversion barrier for *N*-methylpyrrolidine (five-member) and N-methypiperidine (six-member).[68] Ring inversion, the other possible internal motion, can in principle influence the k_{nr} values of the systems. However, since the linear amines are devoid of this particular type of motion, a common mechanism, seeking an explanation on the difference of the k_{nr} values of all the systems, cannot involve this particular type of motion.

One is required to address the influence of the solvent on the k_{nr} values of the systems. As stated earlier, the inversion of the amino nitrogen passes through a transition state involving a planar nitrogen. In the present EDA systems, this transition state is clearly more polar than the initial (or the final) conformation of the amine. Hence, the transition state is expected to be stabilized much more than the initial state in a polar solvent. This will lower the barrier to N-inversion process in a polar media.

What we find quite interesting is the similarity of the photophysical behavior of these systems and NBD derivatives we studied earlier.[14] In both cases, N-inversion seems to be a more acceptable mechanism of nonradiative relaxation process than the internal rotation.

The fluorescence decay behavior of the systems suggest that a second state comes in close proximity with the ICT state in the polar environment. At this point, we are unable to comment on the nature of this second state and its influence on the nonradiative deativation process. Since the width of the fluorescence spectra of a given system in polar media is very similar to that in nonpolar environment and the fluorescence decay parameters obtained at the two ends of the spectra are quite similar, we conclude that the emission is essentially originating from one state (ICT) which comes in equilibrium with another state in polar media.

Conclusion. The spectral and photophysical behavior of several structurally similar 4-amino-1,8-naphthalimides have been studied. A minor variation of the amino functionality, the electron donor component in these EDA molecules, leads to considerable changes in the spectral response and fluorescence

efficiency of the systems. The energetics of the Franck Condon state of these molecules is primarily governed by the ground-state conformation of the amino moiety rather than by its electron-donating ability. The fluorescence efficiency of the systems is strongly dependent on the length of the alkyl chain of the dialkylamino moiety in the linear amines and on the ring size containing the amino nitrogen in the cyclic amines. A faster nonradiative deactivation of the fluorescent state of the systems is observed for systems containing the higher members of the dialkylamino group and higher ring systems. It is concluded that nitrogen inversion at the amino group acts as a nonradiative deactivation pathway for the current systems.

Acknowledgment. This work is supported by a grant from the Department of Science and Technology (DST), Government of India. The fellowship to S.S. was provided by the University Grants Commission. The authors also like to acknowledge the National Single Crystal Diffractometer Facility of University of Hyderabad (established by DST) for the crystal structures. The authors like to thank Mr. Satyanarayan Pal and Dr. S. Pal for cyclic voltammetric measurements.

References and Notes

(1) Michel-Beyerle, M. E. *The Reaction Centre of Photosynthetic Bacteria*; Springer-Verlag: Berlin, 1995.
(2) Diner, B. A.; Babcock, G. T. In *Structure, Dynamics, and Energy Conversion Efficiency in Photosystem II*; Diner, B. A., Babcock, G. T., Eds.; Kluwer: Dordrecht, 1996; p 213.
(3) Bard, A.; Fox, M. A. *Acc. Chem. Res.* **1995**, *28*, 141.
(4) Meyer, T. J. *Acc. Chem. Res.* **1989**, *22*, 163.
(5) Wasielewski, M. R. *Chem. Rev.* **1992**, *92*, 435.
(6) Nandi, N.; Bhattacharyya, K.; Bagchi, B. *Chem. Rev.* **2000**, *100*, 2013.
(7) Chemla, D. S.; Zyss, J. *Nonlinear optical properties of organic molecules and crystals*; Academic Press: New York, 1987.
(8) Maeda, M. *Laser Dyes*; Academic Press: New York, 1984.
(9) Kalyanasundaram, K. *Photochemistry in microheterogeneous systems*; Academic Press: New York, 1987.
(10) Saroja, G.; Ramachandram, B.; Saha, S.; Samanta, A. *J. Phys. Chem. B* **1999**, *103*, 2906.
(11) Jones, G., II; Jackson, W. R.; Choi, C. Y.; Bergmark, W. R. *J. Phys. Chem.* **1985**, *89*, 294.
(12) Gompel, J. A. V.; Schuster, G. B. *J. Phys. Chem.* **1989**, *93*, 1292.
(13) Rechthaler, K.; Köhler, G. *Chem. Phys.* **1994**, *189*, 99.
(14) Saha, S.; Samanta, A. *J. Phys. Chem. A.* **1998**, *102*, 7903.
(15) Saroja, G.; Sankaran, N. B.; Samanta, A. *Chem. Phys. Lett.* **1996**, *249*, 392.
(16) Soujanya, T.; Fessenden, R. W.; Samanta, A. *J. Phys. Chem.* **1996**, *100*, 3507.
(17) Grabowski, Z. R.; Rotkiewicz, K.; Siemiarczuk, A.; Cowley, D. J.; Baumann, W. *Nouv. J. Chim.* **1979**, *3*, 443.
(18) Mareshal, E. *Prog. Org. Coatings* **1982**, 251.
(19) Settimo, A. D.; Primofiore, G.; Ferrarini, P. L.; Ferretti, M.; Barili, P. L.; Tellini, N.; Bianchini, P. *Eur. J. Med. Chem.* **1989**, *24*, 263.
(20) Kireshenbaun, M. R.; Chen, S.-F.; Behrens, C. H.; Papp, L. M.; Stafford, M. M.; Sun, J.-H.; Behrens, D. L.; Fredricks, J. R.; Polkus, S. T.; Sipple, P.; Patten, A. D.; Dexter, D.; Seitz, S. P.; Gross, J. L. *Cancer Res.* **1994**, *54*, 2199.
(21) Brana, M. F.; Castellano, J. M.; Roldan, C. M.; Santos, A.; Vazquez, D.; Jimenez, A. *Cancer Chemother. Pharmacol.* **1980**, *4*, 61.
(22) Brana, M. F.; Sanz, A. M.; Castellano, J. M.; Roldan, C. R.; Roldan, C. *J. Med. Chem. Chim. Ther.* **1981**, *16*, 207.
(23) Rideout, D.; Schinazi, R.; Pauza, C. D.; Lovelace, K.; Chiang, L. C.; Calogeropoulou, T.; McCarthy, M.; Elder, J. H. *J. Cell. Biochem.* **1993**, *51*, 446.
(24) Stewart, W. W. *Nature* **1981**, *292*, 17.
(25) Saito, I. *Pure Appl. Chem.* **1992**, *64*, 1305.
(26) Bailly, C.; Brana, M.; Waring, M. J. *Eur. J. Biochem.* **1996**, *240*, 195.
(27) Dorlars, A.; Schellhammer, C.-W.; Schroeder, J. *Angew. Chem., Int. Ed. Engl.* **1975**, *14*, 665.
(28) Martynski, T.; Mykowska, K.; Bauman, D. *J. Mol. Struct.* **1994**, *325*, 161.
(29) Marling, J. B.; Gregg, D. W.; Thomas, S. J. *J. Quant. Electron.* **1970**, *6*, 570.
(30) Marling, J. B.; Hawley, J. G.; Liston, E. M.; Grant, B. *Appl. Opt.* **1974**, *13*, 2317.
(31) Brochsztain, S.; Rodrigues, M. A.; Politi, M. J. *J. Photochem. Photobiol., A* **1997**, *107*, 195.
(32) Nemes, P.; Demeter, A.; Biczok, L.; Berces, T.; Wintgens, V.; Valat, P.; Kossanyi, J. *J. Photochem. Photobiol., A* **1998**, *113*, 225.
(33) Wintgens, V.; Valat, P.; Kossanyi, J.; Demeter, A.; Biczok, L.; Berces, T. *J. Photochem. Photobiol., A* **1996**, *93*, 109.
(34) Wintgens, V.; Valat, P.; Kossanyi, J.; Demeter, A.; Biczok, L.; Berces, T. *New J. Chem.* **1996**, *20*, 1149.
(35) Demeter, A.; Biczok, L.; Berces, T.; Wintgens, V.; Valat, P.; Kossanyi, J. *J. Phys. Chem.* **1993**, *97*, 3217.
(36) Demeter, A.; Berces, T.; Biczok, L.; Wintgens, V.; Valat, P.; Kossanyi, J. *J. Phys. Chem.* **1996**, *100*, 2001.
(37) Valat, P.; Wintgens, V.; Kossanyi, J.; Biczok, L.; Demeter, A.; Berces, T. *J. Am. Chem. Soc.* **1992**, *114*, 946.
(38) Yuan, D.; Brown, R. G. *J. Chem. Res., Miniprint* **1994**, 2337.
(39) Yuan, D. W.; Brown, R. G. *J. Phys. Chem. A* **1997**, *101*, 3461.
(40) Mitchell, K.-A.; Brown, R. G.; Dongwu, Y.; Chang, S.; Utecht, R. E.; Lewis, D. E. *J. Photochem. Photobiol., A* **1998**, *115*, 157.
(41) Pardo, A.; Poyato, M.; Martin, E. *J. Photochem.* **1986**, *36*, 323.
(42) Pardo, A.; Martin, E.; Poyato, J. M. L.; Camacho, J. J.; Brana, M. F.; Castellano, J. M. *J. Photochem. Photobiol., A* **1987**, *41*, 69.
(43) Pardo, A.; Poyato, J. M. L.; Martin, E.; Camacho, J. J.; Reyman, D. *J. Lumin.* **1990**, *46*, 381.
(44) Pardo, A.; Martin, E.; Poyato, J. M. L.; Camacho, J. J.; Guerra, J. M.; Weigand, R.; Brana, M. F.; Castellano, J. M. *J. Photochem. Photobiol., A* **1989**, *48*, 259.
(45) Samanta, A.; Saroja, G. *J. Photochem. Photobiol., A* **1994**, *84*, 19.
(46) Samanta, A.; Ramachandram, B.; Saroja, G. *J. Photochem. Photobiol., A* **1996**, *101*, 29.
(47) Ramachandram, B.; Saroja, G.; Sankaran, N. B.; Samanta, A. *J. Phys. Chem. B* **2000**, *104*, 11824.
(48) Aveline, B. M.; Matsugo, S.; Redmond, R. W. *J. Am. Chem. Soc.* **1997**, *119*, 11785.
(49) Dmitruk, S. L.; Druzhinin, S. I.; Minakova, R. A.; Bedrik, A. I.; Uzhinov, B. M. *Russ. Chem. Bull.* **1997**, *46*, 2027.
(50) Perrin, D. D.; Armarego, W. L. F.; Perrin, D. R. *Purification of Laboratory Chemicals*; Pergamon Press: New York, 1980.
(51) Reichardt, C. *Solvents and Solvent Effects in Organic Chemistry*; VCH: Weinheim, 1988.
(52) Tyman, J.; Ghorbanian, S.; Muir, M.; Tychopoulous, V.; Bruce, I.; Fisher, I. *Synth. Commun.* **1989**, *19*, 179.
(53) Demas, J. N.; Crosby, G. A. *J. Phys. Chem.* **1971**, *75*, 991.
(54) Bevington, P. R. *Data Reduction and Error Analysis for the Physical Sciences*; McGraw-Hill: New York, 1969.
(55) Sheldrick, G. M. *SHELXS-97*: Göttingen, 1990.
(56) Sheldrick, G. M. *SHELXL-97*: Göttingen, 1997.
(57) Rettig, W.; Maus, M. In *Conformational Changes Accompanying Intramolecular Excited States Electron Transfer*; Waluk, J., Ed.; Wiley-VCH: 2000.
(58) Birks, J. B. *Photophysics of Aromatic Molecules*; Wiley-Interscience: New York, 1979.
(59) Alexiou, M. S.; Tychopoulos, V.; Ghorbanian, S.; Tyman, J. H. P.; Brown, R. G.; Brittain, P. I. *J. Chem. Soc., Perkin Trans. 2* **1990**, *2*, 837.
(60) Lippert, V. E. *Z. Elektrochem.* **1957**, *61*, 962.
(61) Mataga, N.; Kaifu, Y.; Koizumi, M. *Bull. Chem. Soc. Jpn.* **1956**, *29*, 465.
(62) Mataga, N. *Bull. Chem. Soc. Jpn.* **1963**, *36*, 654.
(63) Ravi, M.; Samanta, A.; Radhakrishnan, T. P. *J. Phys. Chem.* **1994**, *98*, 9133.
(64) Kosower, E. M. *Acc. Chem. Res.* **1982**, *15*, 259.
(65) Õki, M. *Applications of Dynamic NMR Spectroscopy to Organic Chemistry*; VCH: Deerfield Beach, 1985.
(66) Belostotskii, A. M.; Aped, P.; Hassner, A. *J. Mol. Struct. (THEOCHEM)* **1997**, *398*−*399*, 427.
(67) Lambert, J. B. In *Pyramidal Atomic Inversion*; Allinger, N. L., Eliel, E. L., Eds.; Wiley: New York, 1971; Vol. 6.
(68) Forsyth, D. A.; Zhang, W.; Hanley, J. A. *J. Org. Chem.* **1996**, *61*, 1284.